JOURNAL OF Applied Polymer SCIENCE

Architectural Characteristics of Stochastic Honeycombs Fabricated from Varying Melt Strength Polypropylenes

Megan Hostetter, Glenn D. Hibbard
Department of Materials Science and Engineering, University of Toronto, Toronto, Ontario, Canada M5S 3E4
Correspondence to: G. D. Hibbard (E-mail: glenn.hibbard@utoronto.ca)

ABSTRACT: Stochastic honeycombs are a cellular polymer fabricated through a simple melt-stretching process. In this study, five polypropylenes (PP) with varying rheological properties were used to fabricate stochastic honeycombs over a range of densities. Rheology tests were performed to determine the melt behavior, while micro-CT scans were used as a nondestructive characterization technique to determine the internal architecture. The sandwich structure consists of parallel skins separated by a network of interconnected webs. The cross-sectional area decreased from unit area at the skins to a plateau over the middle third of the honeycomb height where the cross-sectional area and total edge length of the webs were relatively constant. The rheological properties of the polymer were found to determine the web length per unit area, while the starting areal density of the polymer controlled the mid-height cross-sectional area. Other features, such as archways and buttresses, act as secondary structures that support the webs. © 2013 Wiley Periodicals, Inc. J. Appl. Polym. Sci. **2014**, *131*, 40074.

KEYWORDS: thermoplastics; composites; rheology; X-ray

Received 26 July 2013; accepted 19 October 2013
DOI: 10.1002/app.40074

INTRODUCTION

The internal architecture of polymer-based cellular materials is determined in part by the rheological behavior of the polymer in question. For example, when a polymer is expanded from the melt state to a closed cell foam, the stability of the walls is paramount, and two of the most important properties for wall stability are the melt strength[1–3] and the strain hardening ability of the melt.[4–6]

Polypropylene (PP) has been considered as a substitute for other closed cell foams such as polyurethane, polyethylene, and polystyrene, due to its good mechanical strength and relatively high melt temperature.[7,8] Equally important is its recyclability,[9] as polyurethane is a thermoset,[10,11] many polyethylene foams are cross-linked,[11] and polystyrene foam is quite difficult to recycle.[12,13] However, PP performs poorly in foaming and extrusion due to its low melt strength and lack of strain hardening.[4–6,14] The melt strength is related to the limit of the extensibility of the polymer melt,[14] which in turn stabilizes the growth rate of cells during nucleation and is the controlling factor behind cell wall rupture,[9] while strain hardening is a critical factor in membrane stability and also stabilizes the cell walls, preventing them from expanding too quickly and rupturing.[14] The poor melt strength of PP can lead to melt fracture in extrusion,[14] leading to an open cell foam structure.

To resolve this, high melt strength polypropylenes have been developed in a number of different ways, such as melt addition of organo-clay nanocomposites[15,16] or carbon nanotubes,[17,18] melt grafting in the presence of various peroxides,[1,6,19–23] introduction of high molecular weight PE chains,[24] and electron-beam irradiation in the presence of polyfunctional monomers.[4,25–28] Melt grafting and electron-beam irradiation lead to the introduction of long-chain branching (LCB) in PP, which in turn leads to greater entanglement density in the melt and higher melt strength and melt strain hardening.[9,14,29]

Long chain branching in polypropylene has been shown to increase the processability of PP for industrial purposes. For instance, Stange and Münstedt[30,31] studied the rheological properties of LCB PPs and the effect of the LCBs on foaming of PP. They concluded that the presence of branches led to increased cell density and cell diameter in the PP foam, as well as an increased expansion ratio. Similarly, Nam et al.[32] determined that the most important variable in determining foam density was the degree of long-chain branching of the PP, and that lower densities of foam were achievable when using LCB PPs. Finally, Gotsis et al.[33] modified a linear PP to an LCB PP, and improved the processability of the PP in foaming and thermoforming.

The mechanical properties of closed cell foams depend on the internal cellular architecture of the polymer foams, which in turn is controlled by a convolution of processing parameters

Table I. Polymer Properties for Four High Melt Strength PP (PP-1 to PP-4) and One Conventional (Linear) PP (PP-5)

Polymer	T_m (°C)	η_o ($\times 10^4$ Pa s^{-1})	λ (s)	G_c ($\times 10^4$ Pa)	ω_c (rad s^{-1})	*MFI* + (g/10 min)
PP-1	162	3.24 ± 0.24	0.080 ± 0.002	1.62 ± 0.05	12.5 ± 0.4	2.4
PP-2	163	3.31 ± 0.39	0.209 ± 0.093	0.83 ± 0.22	5.3 ± 2.4	2.1
PP-3	163	2.15 ± 0.21	0.036 ± 0.003	2.09 ± 0.01	28.0 ± 2.3	6.0
PP-4	147	3.94 ± 0.18	0.128 ± 0.039	1.64 ± 0.22	8.2 ± 2.5	2.4
PP-5	167	0.48 ± 0.01	0.015 ± 0.001	4.32 ± 0.12	65.7 ± 3.3	12

+ provided by the manufacturer.

and the physical properties of the bulk polymer.[9] This study looks at the effect LCB in PP can have on the internal architecture of a new type of cellular polymer. Stochastic honeycomb sandwich structures can be produced in a simple, low-cost melt-stretching process; their compressive properties are able to match those of commercial PP honeycombs and exceed those of commercial PP foams for a given relative density.[34] The influence of polymer rheology and areal density of the melt on the architecture of stochastic honeycombs was investigated by using four different high melt strength (HMS) polypropylenes and one conventional (control) PP to fabricate stochastic honeycombs by melt-stretching. Parallel-plate rheometry tests were used to characterize the viscoelastic properties of the starting polymer, and X-ray tomography was used to characterize the architecture of the as-fabricated honeycombs.

EXPERIMENTAL

The five polypropylenes used in this study were Daploy WB135 HMS, WB140 HMS, WB180 HMS, WB260 HMS (Borealis, Austria) and Accucomp HP0306L (Aclo, Canada), henceforth referred to, respectively, as PP-1 to PP-5. To complement the manufacturer supplied melt flow index (ASTM Standard D1238[35]), PP-1 to PP-5 were characterized by differential scanning calorimetry (DSC) and parallel plate rheometry. DSC scans were used to determine the melting temperature and define the processing conditions for each polymer. Samples were put through a heat-cool-heat cycle at 10°C min^{-1} between room temperature and 200°C on a Q20 DSC (TA Instruments, USA). The melting temperatures of the five PP types ranged from 147 to 167°C and are summarized in Table I. Parallel-plate viscosity tests were performed on an advanced rheometric expansion system (ARES, TA Instruments, USA) using a dynamic shear test with sample dimensions of 1 mm through-thickness and 25 mm diameter. The test sweeps the angular frequency from $\omega = 0.01$ to 100 rad s^{-1}, with a fixed strain rate of 1% at 1.1 times the melting temperature (T_m). This temperature allowed direct comparison between the rheological properties of the polymers at the fabrication temperature. The stochastic honeycombs were fabricated by first heating each polymer on a metal plate (at 1.1 T_m) until a viscous melt was formed. Plate and polymer were subsequently removed from the furnace and placed in a custom-built press, where a second metal plate was compressed on top of the molten PP with a force of ~500 N. Subsequently the upper plate was raised to the desired height (in this case, 15 mm) at a rate of 5 mm s^{-1} and locked in place. Upon cooling, the sample spontaneously separated from the plates, resulting in an integrated sandwich structure with upper and lower skins separated by a network of interconnected webs. Four samples for each polymer, with relative densities (ρ) ranging from 11 to 18% were then characterized in a Skyscan 1172 micro-CT X-ray scanner (Micro Photonics, USA) at 44 kV source voltage, 188 μA source current, with an exposure of 158 ms and a rotational step size of 0.4°. The radiographs were reconstructed into a series of cross-sections, with a voxel edge length of 35 μm, and binarized to aid the analysis. The cross-sectional slices were then stacked, giving a three-dimensional model of the internal architecture.

RESULTS AND DISCUSSION

Polymer Characterization

Figure 1 plots the results of the parallel-plate rheometry tests, with viscosity (η) given as a function of angular frequency (ω). Zero-shear viscosity (η_o) was determined by extrapolating the low-shear plateau to a hypothetical "zero" shear. This parameter is used as a benchmark to compare the viscosity of polymers tested under different conditions, but at the same temperature.[36] Under the frequency range available, only PP-5 exhibited a plateau at low shear, and thus a true zero-shear viscosity. The η_o values given in Table I are thus the viscosity at 0.01 rad s^{-1}, which is a lower bound estimate for η_o.

For an ideally elastic solid, Hooke's Law applies, so that when the stress is changed, the strain changes immediately, with the

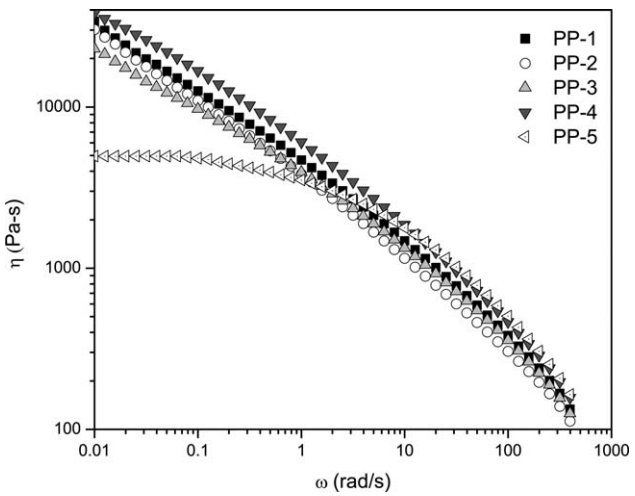

Figure 1. Parallel-plate rheometry results, giving the viscosity (η) as a function of frequency (ω).

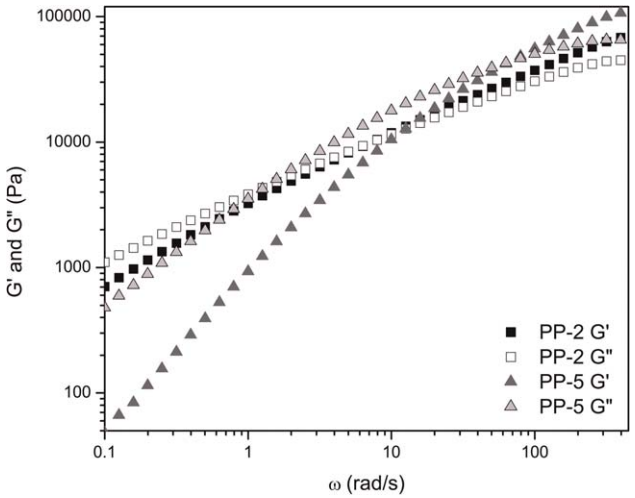

Figure 2. Storage modulus (G') and loss modulus (G'') plotted as a function of frequency (ω) for PP-2 and PP-5.

modulus acting as a constant of proportionality. For a purely viscous solid, the strain is time-dependent and perfectly out of phase with the stress, by $\pi/2$ rad. A viscoelastic solid, as most polymers are, has a phase-lag between 0 and $\pi/2$ rad. The complex modulus [eq. (1)] has an elastic response (the storage modulus, G') that is in phase with the stress, and a viscous response (the loss modulus, G'') that is out of phase with the stress.[29,37]

$$G^* = G' + iG'' \tag{1}$$

Figure 2 plots the storage modulus, G', and the loss modulus, G'', as a function of ω for two polymers (PP-2 and PP-5). At low frequency, G'' is larger than G', implying that the viscous response dominates at low frequency.[29] This allows the characteristic relaxation time, λ, to be determined, which is the timescale separating the predominantly viscous response ($t < \lambda$) from the predominantly elastic response ($t > \lambda$) of the polymer melt. λ is determined by[38]:

$$\lambda = \frac{G'(\omega)}{G''(\omega)\omega} \tag{2}$$

from which it can be seen that $\lambda = \omega^{-1}$ where G' and G'' intersect. This gives the λ values given in Table I.

Figure 3 illustrates the relationship between the two components of the complex viscosity, η' and η", where[38]:

$$\eta'(\omega) = \frac{G''(\omega)}{\omega} \tag{3a}$$

$$\eta''(\omega) = \frac{G'(\omega)}{\omega} \tag{3b}$$

From here, it can be seen that the curves for PP-1 to PP-4 exhibit a change in slope after the second derivative goes through an inflection point at higher η'. This is typically seen for long chain branching in PP, while the semicircular curve for PP-5 is indicative of a linear PP.[1,23]

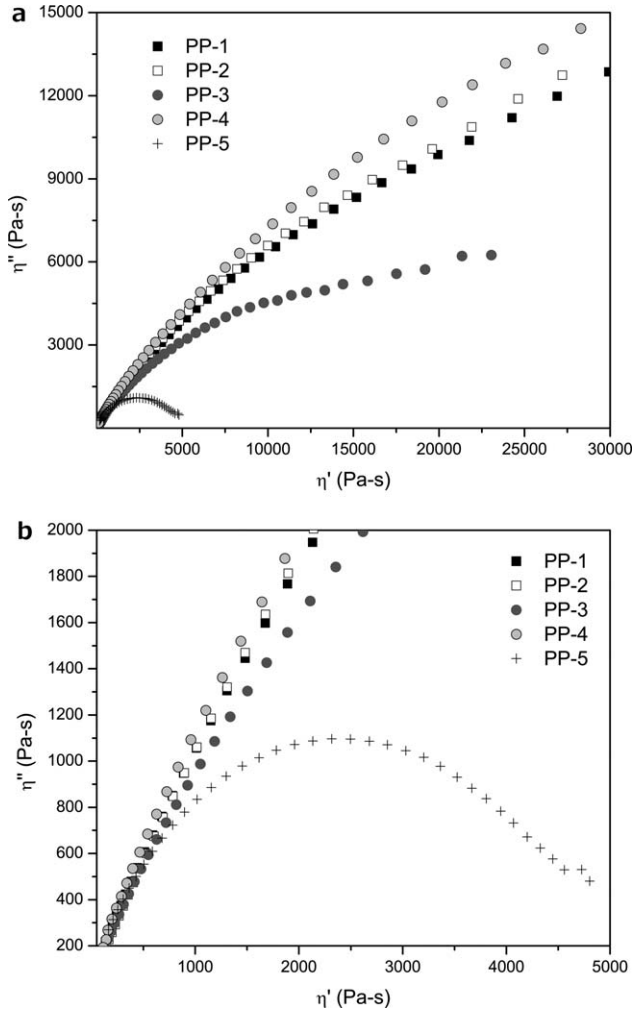

Figure 3. The two components of complex viscosity (η' and η'') from parallel plate rheology tests: the curves for PP-1, PP-2, PP-3, and PP-4 each exhibit a linear portion followed by an increase in slope. This implies that long-chain branching is present in the polymers. PP-5 exhibits a semicircular curve, indicating a linear polymer.[1,23]

The crossover point between the storage and loss moduli (ω_c, G_c) in Figure 2 gives some information about the breadth of the molecular weight distribution (MWD), and about the weight-average molecular weight (M_w). A larger crossover modulus, G_c, implies a narrower MWD, and a lower G_c implies a broader MWD. Similarly, if the crossover occurs at lower frequency, this implies a larger M_w.[39] From these values (Table I) it can be seen that PP-5, the linear PP, has the narrowest MWD and the lowest M_w. PP-2, on the other hand, has the broadest MWD and the highest M_w.

The rheometric data can be compared to the manufacturer supplied melt flow index (MFI). MFI is defined as the mass of polymer passing through a cylinder of set dimensions under a given load and fixed temperature (2.16 kg and 230°C for PP) in ten minutes, and so is reported in g/10 min, after ASTM Standard D1238.[35] It is expected that higher viscosity would lead to less polymer flowing through the cylinder, and vice versa, and indeed it has been found that MFI generally has an inverse

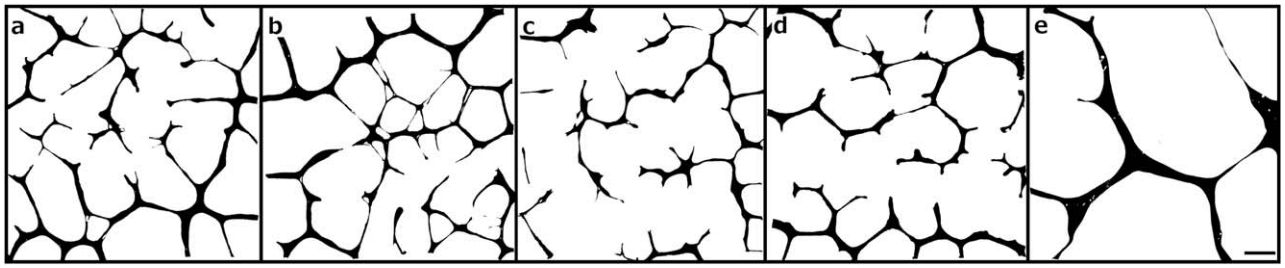

Figure 4. Mid-height cross-sections for PP-1 (a), PP-2 (b), PP-3 (c), PP-4 (d), and PP-5 (e), each having a nominal density of ~20%. The scale bar in part (e) represents a length of 5 mm and applies to each figure.

relationship with η_o.[38] However, η_o is sensitive to both branching and molecular weight distribution,[38] leading to differences between the viscosities of PP-1 and PP-4, even though these two polymers have the same MFI (Table I).

Architectural Characterization

The varying rheological properties of the five polypropylenes under consideration lead to differences in the self-assembled internal architecture of the as-fabricated stochastic honeycombs. The initial areal density of polymer before fabrication (i.e., the mass per unit area before stretching) also affects the architecture, and in turn the mechanical properties.[34] Finally, the structure also varies in the through-thickness direction, with the formation of various types of web defects. Variations in local structure due to the starting polymer type, areal density, and position are discussed below.

Figure 4 presents mid-height cross-sections for the five different polypropylenes at a nominal relative density of ~20%. The four HMS PP samples are comparable, while PP-5 has a much less integrated structure. Similar to the case of melt fracture during conventional foaming, for relative densities below ~20%, the webs for PP-5 (the linear PP) tended to fail, with the molten polymer flowing back to the skins. Although the branched morphology of the webs of each stochastic honeycomb type was comparable, there were fewer, thicker webs for the linear PP.

The normalized cross-sectional areas for each sample were plotted as a function of position, from bottom to top, and are shown in Figure 5. PP-1 to PP-4 all had similar curves, with an initially steep transition from unit area fraction at the skins to the central third of the sample, at which point a relatively constant plateau developed. In the plateau, an average normalized cross-sectional area ($A_c = A_{web}/A_{total}$) could be determined, where the average was taken over the central third of the sample height and the standard deviation was taken as the variation over the same. The web length per unit area within the cross-section ($l_c = l_{web}/A_{total}$) could also be determined over the plateau, and like the area, the length of the webs was nearly constant over the middle third of the specimens (Table II). It is important to note that while PP-5 had a similar density and cross-sectional area in the plateau to the four HMS PPs, the total length of webs was much less (0.07 mm mm^{-2} compared to 0.17 ± 0.02 mm mm^{-2}).

The cross-sectional area fraction over the central third of the honeycomb is an important parameter when considering the mechanical performance because bucking tends to occur where the webs are thinnest and weakest. However, no trend was observed for A_c as a function of the rheological properties: PP-3, PP-4, and PP-5 have similar cross-sectional areas (Table II) but very different viscosities and rheological properties (Table I). In contrast, the total web length per unit area does seem to be determined by the rheological properties of the polymer. Figure 6(a) shows an increase in the web length with increasing zero-shear viscosity, before a plateau is reached at higher values of η_o, while the web length was seen to decrease with increasing crossover frequency [Figure 6(b)]. Crossover frequency is largely determined by the relative molecular weight, with a lower

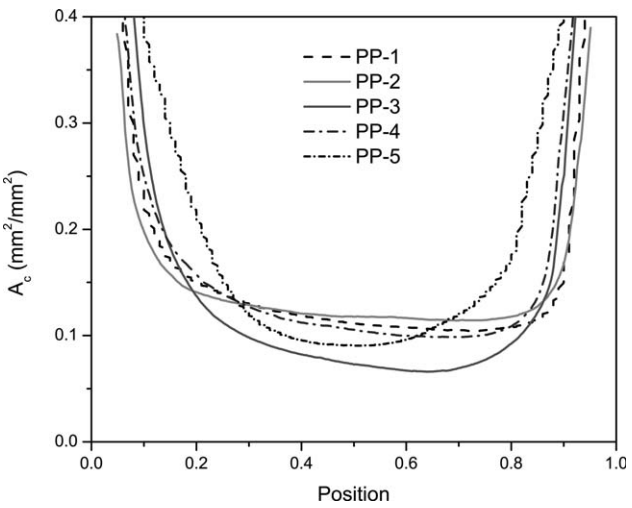

Figure 5. Cross-sectional area fraction as a function of position in the sample (from bottom to top) corresponding to the samples in Figure 4.

Table II. Cross-sectional Area Fraction and Web Length per Unit Area Over the Central Third of the Stochastic Honeycomb Samples (ρ ~20%)

Polymer	Cross-sectional area fraction A_c (mm^2 mm^{-2})	Normalized length of webs l_c (mm mm^{-2})
PP-1	0.113 ± 0.005	0.195 ± 0.007
PP-2	0.118 ± 0.003	0.200 ± 0.003
PP-3	0.074 ± 0.007	0.147 ± 0.004
PP-4	0.086 ± 0.006	0.172 ± 0.013
PP-5	0.095 ± 0.005	0.071 ± 0.001

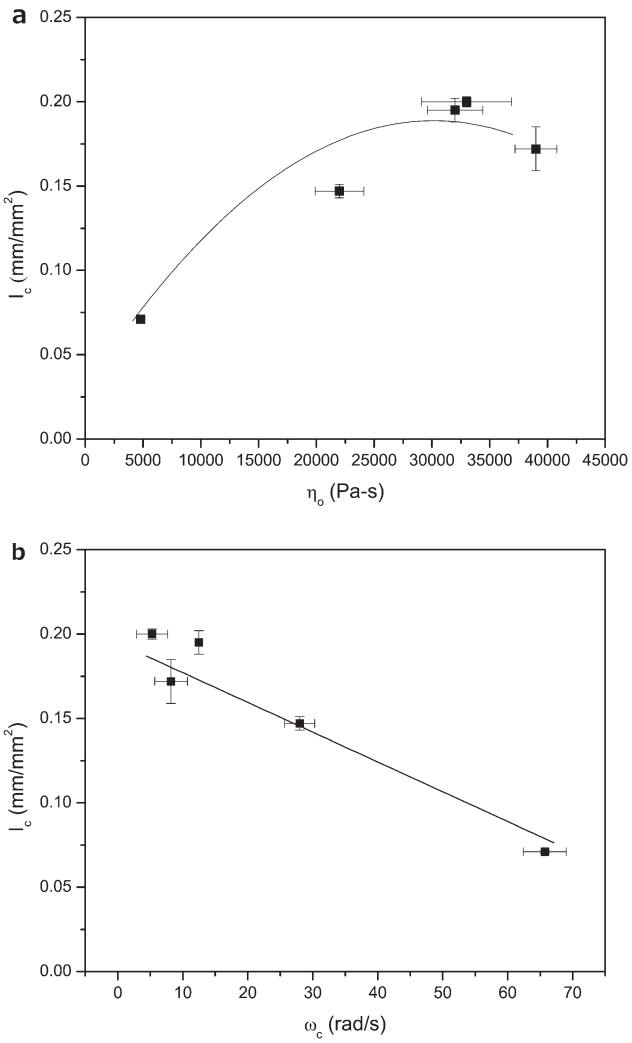

Figure 6. Cross-sectional web length per unit area (at a nominal relative density of ~20%) plotted as a function of zero-shear viscosity (a) and crossover frequency (b).

crossover frequency implying higher M_w. On the other hand, the presence of branching implies a greater entanglement density in the HMS PP than the linear PP, and increasing M_w (or decreasing ω_c) implies increasing entanglement density as well.[39] It may therefore be the case that a certain local density of entanglement points need to be activated during melt stretching in order to create each new web. If there are more entanglements grouped closer together, the resulting melt-stretched architecture will have a greater number of relatively short webs, leading to a greater total web length. In contrast, if there are fewer entanglements, the webs will be longer and fewer in number, as seen with PP-5.

In addition to the rheological properties, the starting areal density before melt stretching also affects the resultant architecture. Figure 7 shows mid-height cross-sections for PP-3 at overall relative densities of $\rho = 10$, 13, 16, and 18% (corresponding to initial areal densities of 0.14, 0.18, 0.21, and 0.25 g cm^{-2}, respectively, before melt stretching to a height of 15 mm). The mid-height web area fraction increases linearly with the overall relative density, from 0.031 ± 0.005 at 10% to 0.074 ± 0.007 at 18%. This leads to the question of whether the mid-height area fraction increases with relative density due to an increase in the web length or the web thickness. Some insight into this question can be obtained by plotting the cross-sectional area (A_c) for PP-2 and PP-3 as a function of areal density in Figure 8. For areal density increases of 50 and 80%, the mid-height web area fractions increased by 50 and 150% for PP-2 and PP-3, respectively. On the other hand, the normalized lengths were within 10 and 15% of the mean value for PP-2 and PP-3. Thus, the cross-sectional area fraction increases linearly with density, while the web length is nearly constant. This implies that as the density increases, the webs generally become thicker, as opposed to becoming more numerous. It was seen previously that polymer entanglement, as indicated by the viscosity and relative molecular weight, affects the total length of webs; here it is seen that the mid-specimen cross-sectional area has a nearly linear dependence on the amount of material present for a given stretching height.

More subtle characteristics of the cellular architecture can be seen by examining a particular sample in more depth. Figure 9 plots the normalized cross-sectional area as a function of position for PP-3 at a relative density of 13%. The transition from the relatively constant middle plateau (a) to the fully dense outer skins begins gradually (b) before steeply increasing through a linear area fraction increase (c–e). Sections through the core at each of these positions are shown in Figure 10. By comparing sequential sections through the sample height it is possible to identify several distinct types of web defects: archways between incomplete webs, buttresses supporting some webs near the skin, and air pockets, or voids, in the thicker portions of the webs. Archways are partial webs that do not stretch

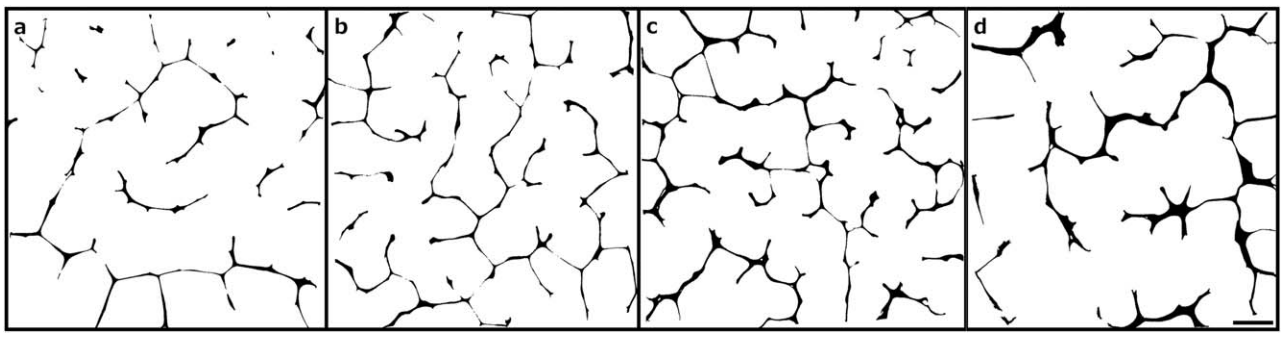

Figure 7. Mid-height cross-sections of PP-3 at $\rho = 10\%$ (a), 13% (b), 16% (c), and 18% (d). The scale bar in (d) is 5 mm and applies to all images.

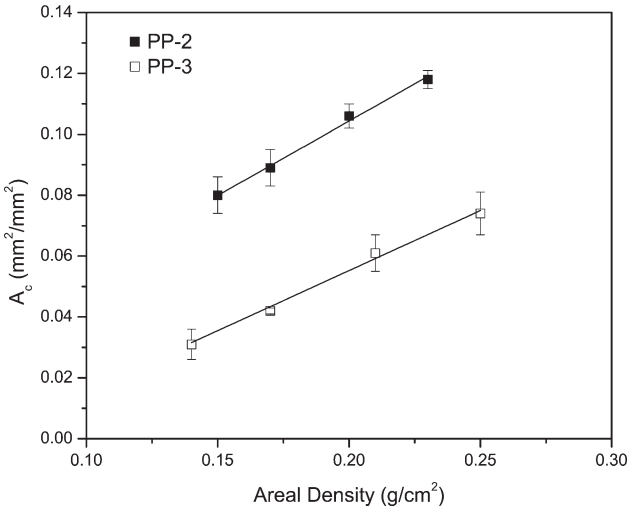

Figure 8. Mid-height cross-sectional area fraction of PP-2 and PP-3 as a function of areal density.

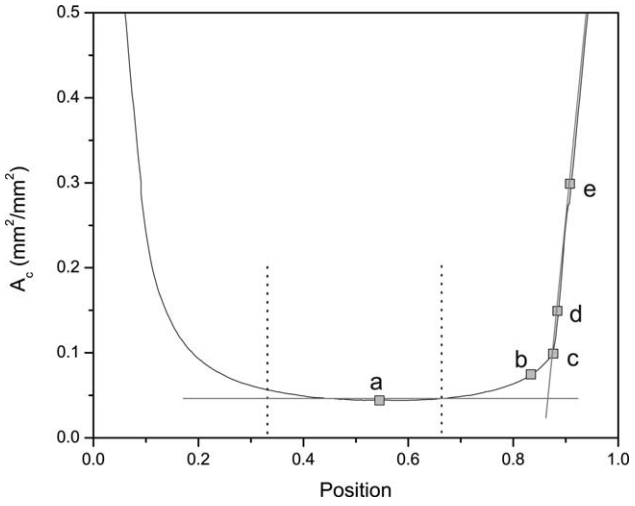

Figure 9. Cross-sectional area fraction plotted as a function of position for PP-3 at $\rho = 13\%$. The central third of the sample was used to determine A_c and l_c.

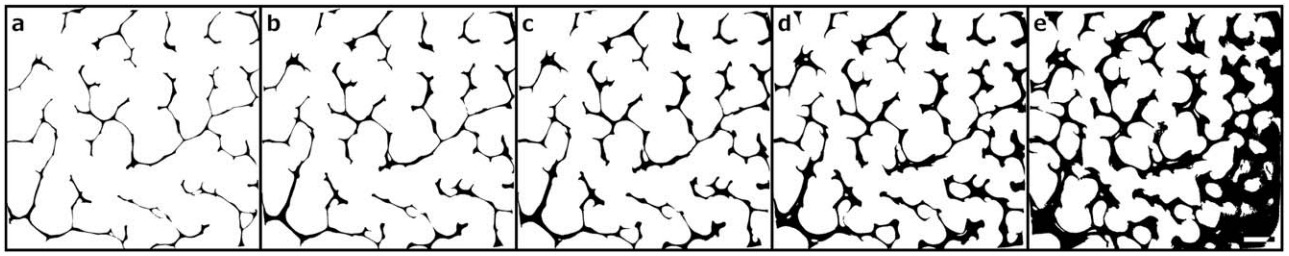

Figure 10. Cross-sectional area slices from positions a–e in Figure 9. The scale bar in (e) is 5 mm and applies to all figures.

entirely from one skin to the other. They can be bounded on one side or on two by adjoining webs, and provide mechanical support to the adjoining webs even though they do not provide a direct through-thickness path for load transmission. Figure 11 shows an example of an archway, with a 3D representation and three horizontal cross-sections through the archway. Buttresses are small, partial webs that support the complete webs. They are located adjacent, and attached, to the skin. When a compressive load is added, they act to resist web buckling and rotation. Figure 12 shows an example of two buttresses, with a 3D representation and three horizontal cross-sections through the webs.

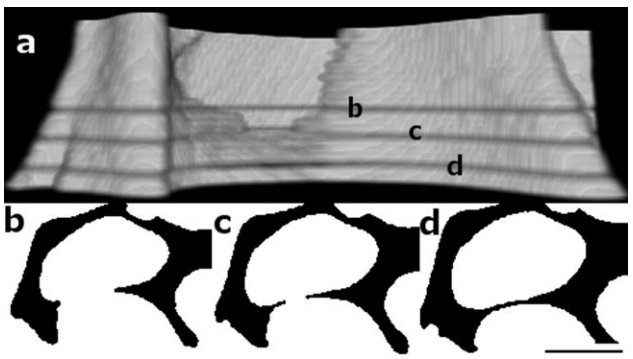

Figure 11. Archway defect in PP-3 ($\rho = 13\%$) shown in a 3D compilation image (a), with horizontal lines marking the position of the cross-sections. The cross-section indicated by the top line is shown in (b), the center line is (c) and the lowest line is (d). The scale bar is 2 mm and applies to (b)–(d).

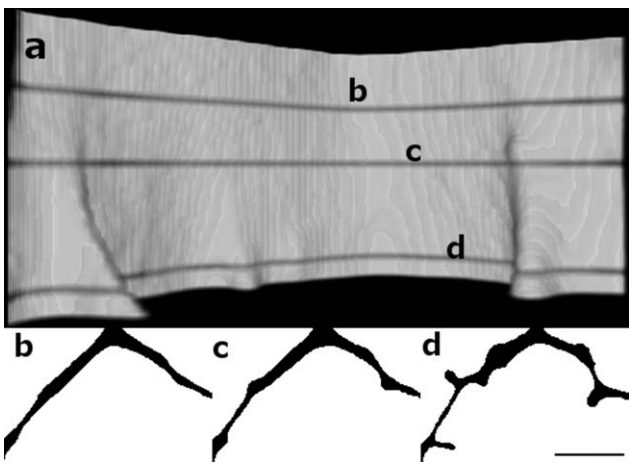

Figure 12. Buttress defect in PP-1 ($\rho = 11\%$) shown in 3D compilation image (a), with horizontal lines marking the position of the cross-sections. The cross-section indicated by the top line is shown in (b), the center line is (c) and the lowest line is (d). The scale bar is 2 mm and applies to (b)–(d).

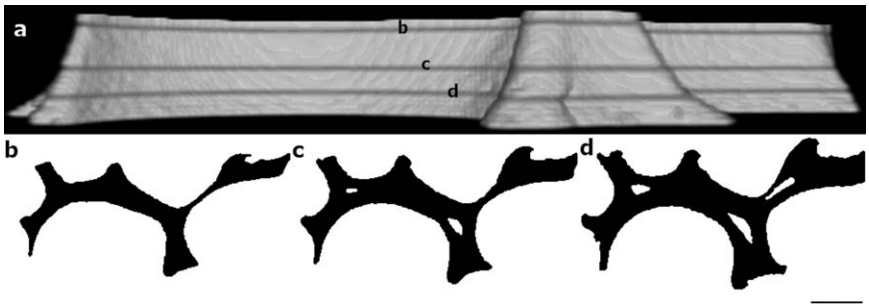

Figure 13. Void defects in PP-3 ($\rho = 13\%$) shown in a 3D compilation image (a), and in three separate cross-sectional slices (b)–(d). The scale bar is 2 mm and applies to (b)–(d).

Figure 13 shows an example of three voids in a web from PP-3 ($\rho = 13\%$), with a 3D representation and three horizontal cross-sections through the voids. Voids generally occur near the top or bottom of the sample where the webs are thicker. For PP-3, the total volume of air pockets in the samples increased from 0.25 to 0.60 cm^3 as the density increased from 10 to 18%. PP-1, PP-2, and PP-4 have a higher total volume of voids, with volumes ranging from 0.60 to 0.90 cm^3 for densities increasing from $\rho = 11$ to 18%.

All four HMS PP types, and to a certain extent PP-5, exhibited archways. Arches occurred in gaps between webs, and were larger near the mid-height of the structure and smaller near the skin. Buttresses and voids, however, were not distributed uniformly between the stochastic honeycombs fabricated with different polymer types. Buttresses were almost nonexistent in PP-5, and rare in PP-3, the least viscous of the four HMS PP. They were much more common in PP-1, PP-2, and PP-4. Voids were present for each polymer type, but were more common in the least viscous polymers (PP-3 and PP-5). Collectively, these web defects represent a secondary type of structure, superimposed upon the network of continuous webs spanning the distance between opposing skin surfaces.

CONCLUSIONS

Micro-CT characterization of stochastic honeycombs produced over a range of densities and from polypropylenes having a range of rheological parameters, revealed the complex internal architecture of these new materials. Within a given specimen, the structure changed continuously from position to position, but over the central third of the honeycomb height, the cross-sectional area and the total length of webs were nearly constant. For a given polypropylene, the mid-height cross-sectional area was seen to increase linearly with the areal density of the molten polymer before melt stretching. However, the total length of webs was relatively constant over the density range examined. This led to the conclusion that as more polymer was available during melt-stretching, the webs formed tended to be thicker, rather than more numerous. In addition, it was determined that the total length of webs was largely governed by the rheological properties of the polymer. Finally, all of the samples, across all densities and polymer types, showed secondary defects such as archways, buttresses and voids, adding to the complexity of structural characterization.

REFERENCES

1. Su, F.-H.; Huang, H.-X. *Polym. Eng. Sci.* **2010**, *50*, 342.
2. Goyal, S. K. *Plast. Eng.* **1995**, *51*, 25.
3. Dealy, J. M.; Wissbrun, K. F. Melt Rheology and its Role in Plastics Processing: Theory and Applications; Van Nostrand Reinhold: Dordrecht, The Netherlands, **1999**.
4. Sugimoto, M.; Tanaka, T.; Masubuchi, Y.; Takimoto, J.; Koyama, K. *J. Appl. Polym. Sci.* **1999**, *73*, 1493.
5. Lau, H. C.; Bhattacharya, S. N.; Field, G. *J. Polym. Eng. Sci.* **1998**, *38*, 1915.
6. Li, S.; Xiao, M.; Wei, D.; Xiao, H.; Hu, F.; Zheng, A. *Polymer* **2009**, *50*, 6121.
7. .Spitael, P.; Macosko, C. W.; Sahnoune, A. Extensional Rheology of Polypropylene and its Effect on Foaming, in Proceedings of the Society of Plastics Engineers ANTEC 2002, **2002**.
8. Zhang, J.; Kikuchi, N.; Li, V.; Yee, A.; Nusholtz, G. *Int. J. Impact Eng.* **1998**, *21*, 369.
9. Gendron, R., Ed. Thermoplastic Foam Processing: Principles and Applications; CRC Press: Boca Raton, FL, **2005**.
10. Szycher, M. Handbook of Polyurethanes; CRC Press: Boca Raton, FL, **1999**.
11. Landrock, A. H. Handbook of Plastic Foams: Types, Properties, Manufacture and Applications; Noyes Publications: Park Ridge, NJ, **1995**.
12. Ukei, H.; Hirose, T.; Horikawa, S.; Takai, Y.; Taka, M.; Azuma, N.; Ueno, A. *Catal. Today* **2000**, *62*, 67.
13. .Stein, R. S. *Proc. Natl. Acad. Sci. USA* **1992**, *89*, 835.
14. Throne, J. L. Thermoplastic Foam Extrusion: An Introduction; Hanser Gardner Publications: Cincinnati, OH, **2004**.
15. Cassagnau, P. *Polymer* **2008**, *49*, 2183.
16. Bailly, M.; Kontopoulou, M. *Polymer* **2009**, *50*, 2472.
17. Lee, G. W.; Jagannathan, S.; Minus, M. L.; Kumar, S. *Polymer* **2008**, *49*, 1831.
18. Xu, D.; Wang, Z. *Polymer* **2008**, *49*, 330.
19. Graebling, D. *Macromolecules* **2002**, *35*, 4602.
20. Tian, J.; Yu, W.; Zhou, C. *Polymer* **2006**, *47*, 7962.
21. Fina, A.; Tabuani, D.; Camino, G. *Polymer* **2009**, *50*, 218.
22. Wong, B.; Baker, W. E. *Polymer* **1997**, *38*, 2781.

23. Zhang, Z.; Wan, D.; Xing, H.; Zhang, Z.; Tan, H.; Wang, L.; Zheng, J.; An, Y.; Tang, T. *Polymer* **2012**, *53*, 121.
24. Sugimoto, M.; Masabuchi, Y.; Takimoto, J.; Koyama, K. *J. Polym. Sci. B Polym. Phys.* **2001**, *39*, 2692.
25. Yoshii, F.; Makuuchi, K.; Kikukawa, S.; Tanaka, T.; Saitoh, J.; Koyama, K. *J. Appl. Polym. Sci.* **1996**, *60*, 617.
26. Kurzbeck, S.; Oster, F.; Muünstedt, H.; Nguyen, T. Q.; Gensler, R. *J. Rheol.* **1999**, *43*, 359.
27. Auhl, D.; Stange, J.; Münstedt, H.; Krause, B.; Voigt, D.; Lederer, A.; Lappan, U.; Lunkwitz, K. *Macromolecules* **2004**, *37*, 9465.
28. Krause, B.; Stephen, M.; Volkland, S. *J. Appl. Polym. Sci.* **2006**, *99*, 260.
29. Deshpande, A. P.; Krishnan, J. M.; Kumar, S., Ed. Rheology of Complex Fluids; Springer: New York, NY, **2010**.
30. Stange, J.; Münstedt, H. *J. Cell. Plast.* **2006**, *42*, 445.
31. Stange, J.; Muünstedt, H. *J. Rheol.* **2006**, *50*, 907.
32. Nam, G. J.; Yoo, J. H.; Lee, J. W. *J. Appl. Polym. Sci.* **2005**, *96*, 1793.
33. Gotsis, A. D.; Zeevenhoven, B. L. F.; Hogt, A. H. *Polym. Eng. Sci.* **2004**, *44*, 973.
34. Hostetter, M.; Cordner, B.; Hibbard, G. D. *Comp. B Eng.* **2012**, *43*, 1024.
35. ASTM D1238. ASTM D1238 Standard Test Method for Melt Flow Rates of Thermoplastics by Extrusion Plastometer. ASTM International **2004**.
36. Fried, J. R. Polymer Science and Technology; Prentice Hall PTR: Upper Saddle River, NJ, **2003**.
37. Margolis, J. M., Ed. Engineering Plastics Handbook: Thermoplastics, Properties and Applications; McGraw-Hill: New York, NY, **2006**.
38. Shenoy, A.; Saini, D. R. Thermoplastic Melt Rheology and Processing; Marcel Dekker, Inc.: New York, NY, **1996**.
39. Dealy, J. M.; Larson, R. G. Structure and Rheology of Molten Polymers: From Structure To Flow Behavior and Back Again; Hanser Gardner Publications: Cincinnati, OH, **2006**.